Journal of Solid State Chemistry 182 (2009) 2409–2416

Contents lists available at ScienceDirect

Journal of Solid State Chemistry

journal homepage: www.elsevier.com/locate/jssc

Reinvestigation of the Fe-rich part of the pseudo-binary system SrO–Fe_2O_3

N. Langhof [a], D. Seifert [b], M. Göbbels [a], J. Töpfer [b,*]

[a] Friedrich-Alexander-University Erlangen-Nuremberg, GeoZentrum Nordbayern, Mineralogy, Schloßgarten 5a, 91054 Erlangen, Germany
[b] University of Applied Sciences Jena, Department of Science and Technology, Carl-Zeiss-Promenade 2, 07745 Jena, Germany

ARTICLE INFO

Article history:
Received 19 March 2009
Received in revised form
15 May 2009
Accepted 24 May 2009
Available online 3 June 2009

Keywords:
Hexagonal ferrites
Hard magnets
Phase diagram
Sr–Fe–O

ABSTRACT

The phase relations in the Fe-rich part of the pseudo-binary system SrO–Fe_2O_3 (>33 mol% Fe_2O_3) were reinvestigated between 800 and 1500 °C in air. A combination of microscopy, electron probe microanalysis, powder X-ray diffraction and thermal analysis was used to determine phase relations, crystal structure parameters and phase transition temperatures. *M*-type hexagonal ferrite $SrFe_{12}O_{19}$ (85.71 mol% Fe_2O_3) is stable up to 1410 °C. No indication of a significant phase width was found; $Sr_4Fe_6O_{13\pm\delta}$ appears as a second phase in compositions with <85.71 ±0.2 mol% Fe_2O_3. $Sr_4Fe_6O_{13\pm\delta}$ itself is stable between 800 and 1250 °C. Two other hexagonal ferrites were found to exist at high temperatures only: *W*-type $SrFe_2^{2+}Fe_{16}^{3+}O_{27}$ is stable between 1350 and 1440 °C and *X*-type ferrite $Sr_2Fe_2^{2+}Fe_{28}^{3+}O_{46}$ between 1350 and 1420 °C, respectively, which is shown here for the first time. These findings in combination with previously published data were used to derive a corrected phase diagram of the Fe-rich part of the pseudo-binary system SrO–Fe_2O_3.

1. Introduction

The introduction of Ba- or Sr-hexaferrites (Ba/Sr)$Fe_{12}O_{19}$ as hard magnetic materials in the 1950s [1] has led to an enormous interest in the alkaline-earth oxide–ferric oxide systems. The first systematic study of the pseudo-binary system SrO–Fe_2O_3 in oxygen was published by Batti [2]. This author reported several compounds to exist on the Sr-rich side of the system: $Sr_3Fe_2O_7$, $SrFeO_3$ and $Sr_7Fe_{10}O_{22}$. In the Fe-rich part of that system the hexagonal *M*-type ferrite $SrFe_{12}O_{19}$ (SF_6) was reported to be stable up to 1448 °C (incongruent melting to form magnetite and a liquid). A few years later, Goto et al. [3] reported a study on the system $SrFeO_3$–Fe_2O_3 in air. Theses authors also included the compound $Sr_3Fe_4O_9$ as being stable up to 1225 °C. $SrFe_{12}O_{19}$ was shown to melt incongruently at 1390 °C under formation of $SrFe_{18}O_{27}$ and a liquid. However, significant differences with respect to Ref. [2] were obvious: (i) In Batti's diagram $SrFe_{12}O_{19}$ was referred to as a line compound without any solubility for SrO, whereas Goto described a *M*-type ferrite phase field spanning from the stoichiometric ferrite (85.71 mol% Fe_2O_3) up to 82 mol% at 1195 °C into the Sr-rich direction. The width of this phase field was reported to become smaller with decreasing temperature and to disappear at 1100 °C. This question is of some significance, since all technical hard ferrite compositions are somewhat Sr-rich compared to stoichiometric $SrFe_{12}O_{19}$; typically 84.0–85.0 mol% Fe_2O_3, corresponding to a Fe_2O_3/SrO ratio of $F/S = 5.8$–5.9 (6.0 for stoichiometric SF_6). The question arises whether these Sr-excess hexaferrite compositions are single-phase *M*-type materials or represent two-phase mixtures of $SrFe_{12}O_{19}$ and a Sr-rich second phase. The existence of such a wide ferrite phase field (i.e. large solubility of SrO in SF_6) would, as a consequence, open a discussion on how this excess SrO would be accommodated into the ferrite lattice. Possible point defect mechanisms include the incorporation of additional Sr^{2+} on Sr-sites of the ferrite structure and subsequent formation of Fe- and oxygen vacancies. (ii) In Goto's diagram another hexagonal ferrite $SrFe_{16}O_{27}$ with *W*-type structure was included with a stability region between 1390 and 1420 °C which was not observed at all in Ref. [2]. No other hexagonal ferrites have been reported in both pseudo-binary phase diagrams.

The hexagonal ferrites belong to a family of oxides which are derived from a stacking of close-packed oxygen/barium layers along the hexagonal *c*-axis with an ordering sequence of *S*-, *R*- and *T*-blocks, where *S* is a two-layer building unit $(Fe_6O_8)^{2+}$, *R* is a three-layer block of composition $(SrFe_6O_{11})^{2-}$ and *T* consists of the four-layer unit $Sr_2Fe_8O_{14}$. Combination of *RS* gives the structure of the *M*-type ferrite $SrFe_{12}O_{19}$ which is equivalent to the magnetoplumbite structure of $PbFe_{12}O_{19}$ described by Adelsköld [4]. A stacking sequence RSS or MS results in the *W*-type hexagonal variant $SrMe_2Fe_{16}O_{27}$ and that of RSRSS = MMS in the *X*-type hexagonal ferrite $Sr_2Me_2Fe_{28}O_{46}$. If the *T*-block is included, the *Y*-type hexagonal ferrite $Sr_2Me_2Fe_{12}O_{22}$ is obtained for a combination of *TS*, whereas a stacking of RSTS (or MY) gives the typical structural motif of the *Z*-type structure $Sr_3Me_2Fe_{24}O_{41}$ [5,6].

* Corresponding author. Fax: +49 3641 205451.
E-mail address: joerg.toepfer@fh-jena.de (J. Töpfer).

0022-4596/$ - see front matter © 2009 Elsevier Inc. All rights reserved.
doi:10.1016/j.jssc.2009.05.039

It was shown by Yoshiasa et al. [7] that the stable phase at about 42 mol% Fe_2O_3 is $Sr_4Fe_6O_{13}$. This perosvkite-related material has earned a lot of attention as possible candidate for oxygen separation membranes (e.g. [8]). It's precise crystal structure description lead to the detection of structural incommensurability [9].

Recently, Fossdal et al. [10] reinvestigated the Sr-rich part of the SrO–Fe_2O_3 system. They determined the stability limits of the Ruddlesden-Popper type compounds $Sr_{n+1}Fe_nO_{3n+1}$ with $n = 1$, 2, and 3, of the perovskite solid solutions $Sr_{1\pm x}FeO_{3-\delta}$ and $Sr_4Fe_6O_{13}$ and proposed a corrected version of the SrO-rich part of the phase diagram. Data on the Fe-rich part were taken from Batti [2].

However, some questions remained unanswered that prompted us to reinvestigate the Fe-rich part of the SrO–Fe_2O_3 system (>33 mol% Fe_2O_3). This study is focused on the following issues: (i) is there any solubility of SrO in *M*-type ferrite $SrFe_{12}O_{19}$, (ii) do any other hexagonal Sr-ferrite phases exist and what are their stability limits, and (iii) what is the stability region for $Sr_4Fe_6O_{13\pm\delta}$.

2. Experimental

2.1. Sample preparation

All samples were prepared using the standard ceramic process with $SrCO_3$ (Aldrich) and Fe_2O_3 (Riedel de Haën for set A, TKS-HP for set B) as raw materials. For phase diagram studies a set of samples A with selected compositions (36.0; 47.0; 75.0; 87.5 and 93.0 mol% Fe_2O_3) was prepared by mixing the raw materials in a mortar and calcination at 1100 °C. The obtained powder was milled in a Retsch RS1 vibrating mill. About 500 mg of the samples were placed in small bags made of Pt foil and suspended on Pt wires in a vertical tube furnace and equilibriated at a given temperature between 1200 and 1500 °C for 100 h and then quenched by plunging the sample containers into water. After re-milling the samples were heated again at for several days and quenched. The accuracy of the temperature in the used furnaces and thermocouples was checked to be ±5 °C.

To study the properties of single-phase materials a second set of samples B (batch size 20 g) was synthesized by mixing the raw materials in a polyethylene container with 2-propanol and zirconia balls (diameter 3 mm) for 3 h. After drying the mixture was calcined at 1200 °C for 6 h. The samples were ground with a planetary mill (Pulverisette 5; Fritsch GmbH, Germany) for 8 h in a WC container with water and WC balls (3 mm diameter). This procedure gives powders with a mean particle size of about 1 μm and a specific surface of 1.2 m^2/g. The dried powders were pressed into pellets 10 mm in diameter and sintered at suitable temperatures at 1000–1400 °C in chamber and vertical tube furnaces with commercial Eurotherm electronic temperature controllers. Depending on the temperature and the presence or absence of a melt, equilibration periods of 4 h to 4 weeks were selected. The temperatures were measured by using a Pt6Rh/Pt30Rh thermocouple calibrated against the melting points of gold at 1064.5 °C and diopside ($CaMgSi_2O_6$) at 1393.5 °C corresponding to the IPTS-68 temperature scale. Sintering atmosphere was air and all samples were quenched in water.

2.2. Measurements

Samples of set A were studied by BSE images and characterized by electron probe microanalysis (EPMA—JEOL JXA-8200) employing WDX-mode. The absolute error is assumed to be less than 1.0 mol%.

Samples of set B were studied with powder X-ray diffraction (Siemens D5000 with Cu*K*α radiation; step time 8s; step size 0.02°; 10–70(140°) 2θ). Lattice parameters were refined using the TOPAS R software package (Bruker AXS, Karlsruhe, Germany). The microstructure of polished samples was studied by scanning electron microscopy SEM (DSM 940A, Zeiss, Germany). The specific surface area of the powders A_s was determined by the BET method (Nova 2000, Quantachrome Instruments, Boynton Beach, USA). Thermal analysis (TG, DTA) was carried out with a SETARAM TGA92 system, the samples were heated in air to 1500 °C with a rate of 10 K/min.

Magnetic properties were measured with a Quantum design MPMS SQUID magnetometer. Hysteresis loops were measured at 5 and 298 K. The magnetization at the maximum field of 50 kOe was taken as saturation magnetization M_s.

The Fe^{2+}-concentration was determined by chemical titration after dissolution of the powdered sample in hydrochloric acid under argon. The Fe^{2+} was titrated with a 0.05 N Ce^{4+} solution under a flow of argon with potentiometric detection of the equivalent point. The detection limit of the titration is given by the first drop of Ce^{4+} solution ($V \approx 0.03$ ml) which corresponds to 0.08 wt% Fe^{2+} for 100 mg of a ferrite sample.

3. Results

3.1. Electron probe micro-analysis of multi-phase samples

The phase composition of samples of set A heated at various temperatures in air was analyzed by microscopy and X-ray diffraction. The compositions of individual phases were determined with EPMA. The analytical results of the Fe-rich phases observed in multi-phase compositions after equilibrating samples with total composition of 36.0; 47.0; 75.0, 87.5 and 93.0 mol% Fe_2O_3 at temperatures between 1200 and 1500 °C are summarized in Table 1.

Fig. 1a shows as an example of a Fe-poor composition (starting mixture SF36 with 36.0 mol% Fe_2O_3) a BSE image of a sample sintered at 1245 °C for 24 h consisting of a mixture of the

Table 1
Compositions of Fe-rich phases in the system Sr–Fe–O (1200–1500 °C) measured by EPMA in mol% (also given are standard deviations SD in %).

Compound	Theoretical composition		Measured with electronprobe microanalysis[a]	
	Fe_2O_3 (FeO) (mol%)	SrO	Fe_2O_3 (FeO) (mol%)	SrO
Fe_2O_3	100	0	100	0
SD (%)			1.0	–
Fe_3O_4	50 (50)	0	50 (50)	0
SD (%)			1.0	–
$SrFe_2^{2+}Fe_{16}O_{27}$ (*W*)	72.7 (18.2)	9.1	72.7 (18.4)	8.9
SD (%)			1.2	1.4
$SrFe_2^{2+}Fe_{28}O_{46}$ (*X*)	77.8 (11.1)	11.1	77.8 (11.4)	10.8
SD (%)			0.8	1.3
$SrFe_{12}O_{19}$ (*M*)	85.7	14.3	86.1	13.9
SD (%)			1.0	1.6
$Sr_4Fe_6O_{13\pm\delta}$ ($\delta \approx 0.1$)	42.9	57.1	43.8	56.2
SD (%)			1.2	0.8
$SrFe_6O_{3-\delta}$ (*P*) ($\delta \approx 0.5$)	33.3	66.7	34.3	65.7
SD (%)			1.5	1.5

[a] FeO content resp. Fe^{2+} calculated after [16].

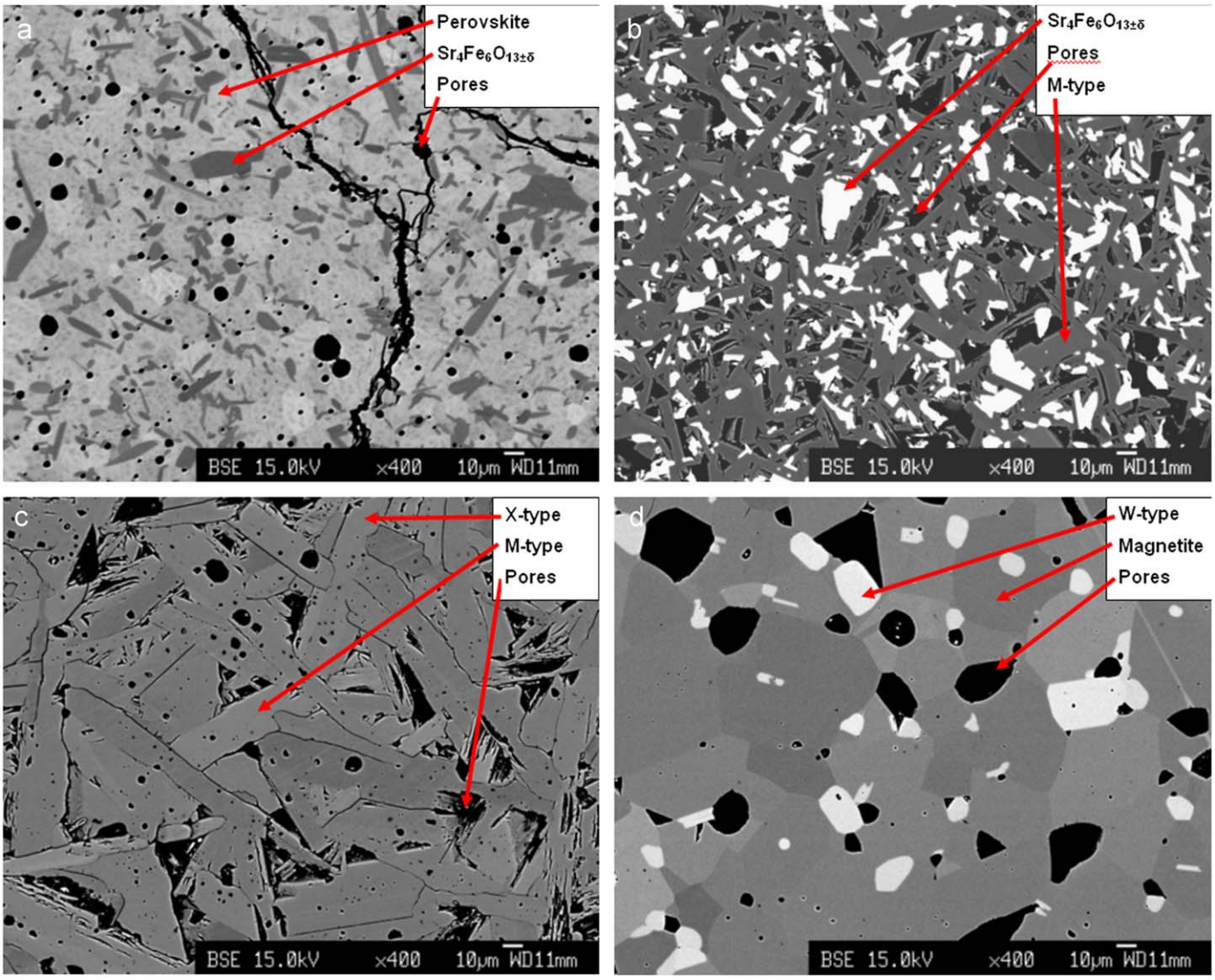

Fig. 1. SEM micrographs of samples with 36.0 mol% Fe_2O_3 sintered for 24 h at 1245 °C (a), with 75.0 mol% Fe_2O_3 sintered for 30 d at 1200 °C (b), with 87.5 mol% Fe_2O_3 sintered for 20 h at 1390 °C (c), and with 93.0 mol% Fe_2O_3 sintered for 24 h at 1390 °C (d).

perovskite $SrFeO_{3-\delta}$ and $Sr_4Fe_6O_{13\pm\delta}$. Fig. 1b shows *M*-type $SrFe_{12}O_{19}$ and $Sr_4Fe_6O_{13\pm\delta}$ as two coexisting phases after firing the starting mixture SF75 with 75 mol% Fe_2O_3 at 1200 °C for 30 days. Above the solidus temperature (1206 °C) samples SF75 contain solidified melt. Starting mixture SF87.5 (87.5 mol% Fe_2O_3) after sintering at 1390 °C for 20 h exhibits *M*-type $SrFe_{12}O_{19}$ in equilibrium with *X*-type $Sr_2Fe_2^{2+}Fe_{28}^{3+}O_{46}$ (Fig. 1c). It is not possible to distinguish both hexagonal ferrites in the BSE image; however, the EPMA results clearly indicate the existence of two different ferrites (Table 1). The Fe-rich mixture SF93 (93 mol% Fe_2O_3) sintered at 1390 °C for 24 h (Fig. 1d) consists of magnetite ($Fe^{2+}Fe_2^{3+}O_4$) and *W*-type $SrFe_2^{2+}Fe_{16}^{3+}O_{27}$ (which appears brighter due to higher average atomic number).

Inspection of the EMPA compositional analysis data (Table 1) of all samples of set A containing *M*-type ferrite $SrFe_{12}O_{19}$ reveals no indication of a significant phase width of that compound. Within the accuracy of the method (±1%) all analyzed data overlap at (85.71 ± 0.86) mol% Fe_2O_3.

Fig. 2a shows a section of the phase diagram between 80 and 100 mol% Fe_2O_3 including the compositions of the three hexagonal ferrites as analyzed by EMPA. Since the average atomic numbers of the hexagonal ferrites are similar (and orientational effects occur) the differentiation of these compounds in the BSE images is difficult. Usually 10 individual EMPA points were analyzed to give one average ferrite composition shown in Fig. 2a. Besides *M*-type $SrFe_{12}O_{19}$ there are two other hexagonal ferrites (*W*- and *X*-type). All ferrites show incongruent melting behavior. Another section of the phase diagram with 33–48 mol% Fe_2O_3 including EMPA results is shown in Fig. 2b. $Sr_4Fe_6O_{13\pm\delta}$ is stable up to 1250 °C. On the Fe-poor side it coexists with a perovskite $Sr_{1\pm x}FeO_{3-\delta}$. The perovskite compositions are somewhat Fe-rich with respect to the stoichiometric composition confirming a significant extend of solid solubility as already reported by Fossdal et al. [10].

3.2. *M*-type hexagonal ferrite

The stoichiometric *M*-type hexagonal ferrite $SrFe_{12}O_{19}$ (85.71 mol% Fe_2O_3; ferric to strontium oxide ratio $F/S = 6$) and SrO-excess compositions with 85.5 ($F/S = 5.89$); 85.2 ($F/S = 5.76$); 85.0 ($F/S = 5.67$) and 84.0 mol% Fe_2O_3 ($F/S = 5.25$), respectively, were synthesized in sample set B. In addition, one iron-excess sample with 87 mol% Fe_2O_3 ($F/S = 6.69$) was prepared. All samples were sintered at 1200 °C for 24 h in air and quenched; according to

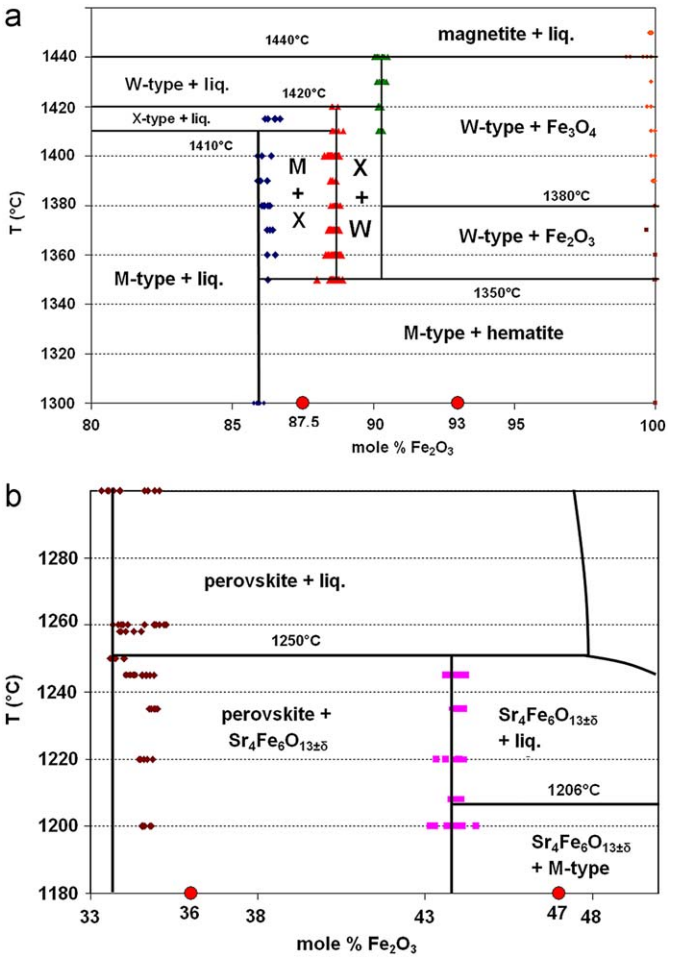

Fig. 2. Sections of the SrO–Fe_2O_3 phase diagram in air with all studied compositions included; 80–100% Fe_2O_3 (a) and 33–48% Fe_2O_3 (b).

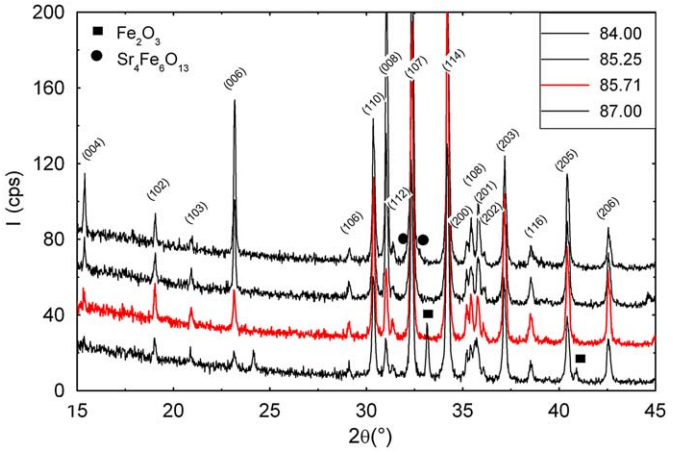

Fig. 3. X-ray diffraction patterns of hexagonal ferrite samples with different compositions (from top to bottom): SrO-excess samples with 84.0 and 85.2 mol% Fe_2O_3, stoichiometric hexaferrite $SrFe_{12}O_{19}$ (85.71 mol% Fe_2O_3) and Fe_2O_3-excess sample with 87 mol% Fe_2O_3 (sintered at 1200 °C for 24 h in air and quenched).

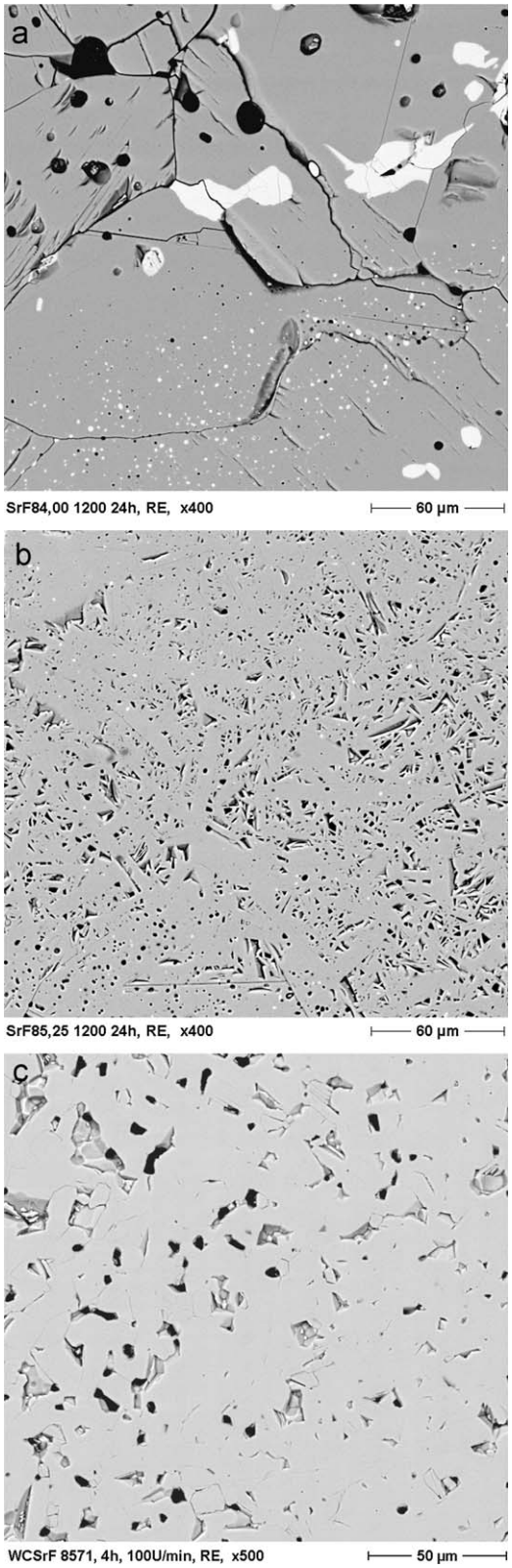

Fig. 4. SEM micrographs of samples with 84.0% (a), 85.2% (b) and 85.7% Fe_2O_3 (c); (gray: hexagonal ferrite; white: Sr-rich phase; dark: pores).

Goto [3] this temperature refers to maximum SrO solubility in the ferrite. XRD patterns (Fig. 3) demonstrate, that the stoichiometric composition (85.7% *F*) is single-phase; all reflections can be indexed within the magnetoplumbite-type structure (SG: $P6_3/mmc$; $z = 2$). As expected, in the sample with 87% *F* haematite is found as second phase besides ferrite. On the other hand, in SrO-excess samples a second phase is detected with XRD for the 84% *F* composition only. The main reflections of $Sr_4Fe_6O_{13}$ can be found as shoulders of the (107) peak of the *M*-type ferrite. The SrO-excess samples were also examined with SEM (Fig. 4). Whereas the sample with 85.7% *F* consists of ferrite grains only (Fig. 4c), in

samples with 84.0–85.2% *F* some grains of a second phase enriched in Sr were detected (Fig. 4a and b). This demonstrates the importance to control the phase composition by microscopy. It is not possible to conclude on a single-phase nature of the investigated ferrite samples by standard X-ray diffraction alone, since either the concentration of second phases is too small to be detectable by routine XRD measurements or the peaks of the second phase overlap with those of the main ferrite phase. In sample 85.5% *F* no second phase was detected either by XRD or SEM. This finding is consistent with the results from the EPMA study described above; within the error of the analytic tools used in this study, the solubility of SrO in $SrFe_{12}O_{19}$ is small and limited to compositions from 85.5 to 85.7 mol% Fe_2O_3. The variation of ferrite lattice parameters as function of composition is shown in Fig. 5. For $SrFe_{12}O_{19}$ (85.7% *F*) unit cell dimensions were refined to $a_0 = 5.8847(2)$ Å and $c_0 = 23.0511(9)$ Å in good agreement with data from other studies [5,11,12]. The lattice parameters of the Sr- and Fe-excess samples do not differ significantly, which is also an indication of the low solubility of SrO in *M*-type hexagonal ferrite.

The thermal behavior of $SrFe_{12}O_{19}$ was studied by thermal analysis between 1200 and 1500 °C (Fig. 6). The TG curve of the stoichiometric sample (85.7% Fe_2O_3) shows a constant mass until at $T > 1350$ °C a series of mass losses signals the decomposition of the *M*-type ferrite; simultaneously a series of three endothermic DTA signals is observed. The first DTA peak with an onset of 1418 °C indicates the incongruent melting of $SrFe_{12}O_{19}$ and formation of *X*-type $Sr_2Fe_2^{2+}Fe_{28}^{3+}O_{46}$ ferrite; a mass loss of 0.5% is indicative of the reduction process. The second peak (onset at 1435 °C) represents the melting of the *X*- and formation of *W*-type hexagonal ferrite $SrFe_2^{2+}Fe_{16}^{3+}O_{27}$. This is also accompanied by liberation of oxygen, a mass loss of 0.3% is observed. The third peak (onset at 1452°) finally signals the incongruent melting of *W*-type ferrite and formation of magnetite $Fe_1^{2+}Fe_2^{3+}O_4$ with a corresponding mass loss of 1.0%. The onsets of the DTA peaks are somewhat higher than the ferrite decomposition temperatures determined in the phase equilibrium studies (Section 3.1.), however, the series of thermal events confirms the phase transformations as proposed in 3.1 and documented in Fig. 2a. For SrO-excess samples the same series of TG steps and DTA peaks is observed (shown for 84% and 85.25% Fe_2O_3 in Fig. 6). The onset temperatures of the DTA peaks do not change compared to stoichiometric $SrFe_{12}O_{19}$ indicating that the composition of the *M*-type ferrite phase has not changed. This confirms the very limited solubility of SrO in $SrFe_{12}O_{19}$. The DTA curve of the composition with 87% Fe_2O_3 (mixture of *M*-type and haematite at $T = 1200$ °C) shows another peak at 1370 °C below the three ferrite phase transformations. This is interpreted as being a signature of the transformation into a mixture of *M* and *X*-ferrite phases.

However, the very limited solubility of SrO in $SrFe_{12}O_{19}$ implies that at $T > 1206$ °C in samples with 84.0% to 85.2% Fe_2O_3 a liquid phase appears. This is reflected in the shrinkage and densification behaviors of SrO-excess $SrFe_{12}O_{19}$. The dilatometric shrinkage curve (Fig. 7) of a SrO-excess sample with 84% Fe_2O_3 exhibits significant shrinkage and a shrinkage rate peak at 1210 °C due to the formation of a liquid phase. In contrast, stoichiometric *M*-type ferrite with 85.71% Fe_2O_3 shrinks at higher temperature with a shrinkage rate maximum at $T = 1370$ °C. In the case of the Fe-excess sample with 87% Fe_2O_3 maximum shrinkage appears at 1350 °C; at that temperature this composition (mixture of SF_6 and haematite) undergoes a solid state transformation into *M*-type and *X*-type ferrites. This shrinkage behavior is also reflected in the densification of green compacts (Fig. 7, inset). Samples with 85.71% and 87.0% *F* display no significant densification after sintering for 4 h at 1200 °C; a continuous increase of density at $T > 1200$ °C is typical of solid state sintering. The samples with 84%, 85.2% and 85.5% *F* show high densities after sintering at around 1200 °C due to liquid phase formation. An increase in sintering temperature does not lead to further densification.

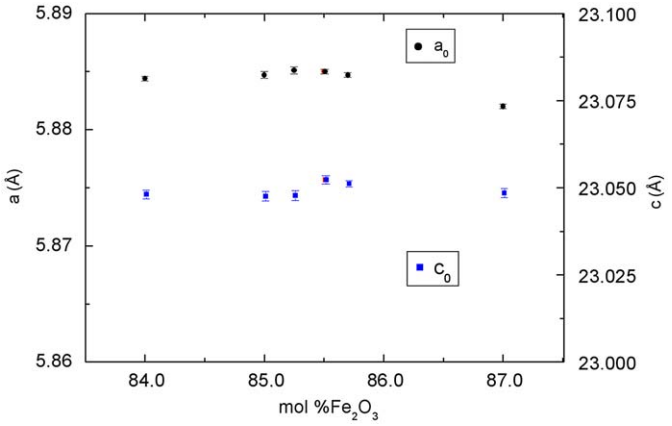

Fig. 5. Variation of lattice parameters as function of composition for samples with 84.0–87.0% Fe_2O_3 (stoichiometric $SrFe_{12}O_{19}$ with 85.7% *F*).

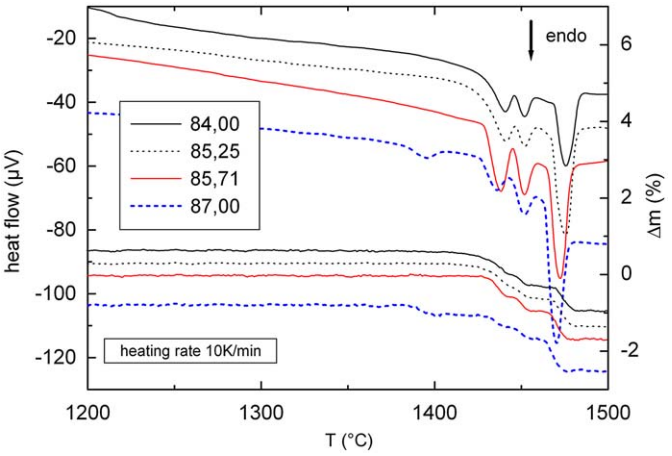

Fig. 6. Thermal analysis curves (TG and DTA) of hexagonal ferrite samples with different compositions (from top to bottom): SrO-excess samples with 84.0 and 85.2 mol% Fe_2O_3, stoichiometric hexaferrite $SrFe_{12}O_{19}$ (85.71 mol% Fe_2O_3) and Fe_2O_3-excess sample with 87 mol% Fe_2O_3 (sintered at 1200 °C for 24 h in air and quenched).

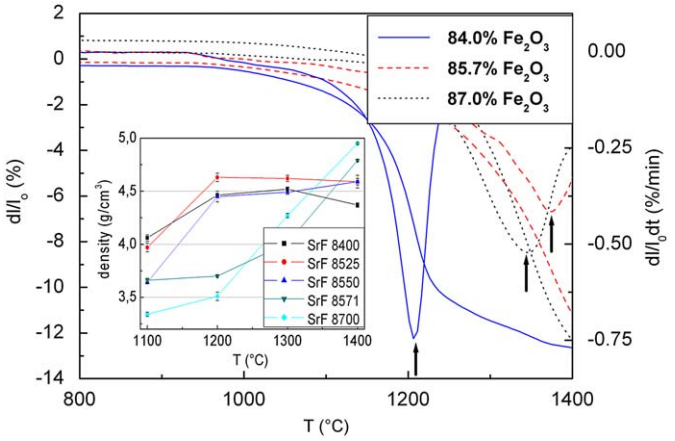

Fig. 7. Dilatometric shrinkage (left axis) and shrinkage rate (right axis) curves of a SrO-excess sample with 84.0 mol% Fe_2O_3, stoichiometric hexaferrite $SrFe_{12}O_{19}$ (85.71 mol% Fe_2O_3) and a Fe_2O_3-excess sample with 87 mol% Fe_2O_3 (sintered at 1200 °C for 24 h in air and quenched), inset: density vs. sintering temperature for samples with 84%, 85.25%, 85.50%, 85.7% and 87% Fe_2O_3.

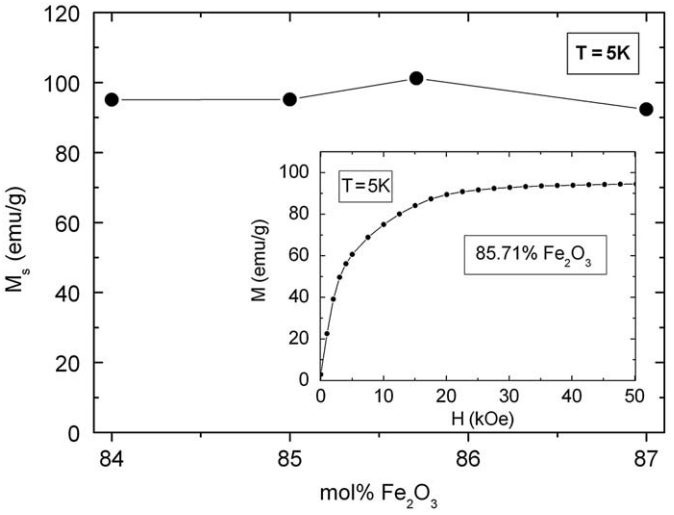

Fig. 8. Saturation magnetization M_s at 5 K as function of composition for samples with 84.0 mol% Fe_2O_3 (SrO-excess), 85.71 mol% Fe_2O_3 (stoichiometric $SrFe_{12}O_{19}$) and 87 mol% Fe_2O_3 (Fe_2O_3-excess); sintered at 1200 °C for 24 h in air and quenched; inset: magnetization at $T = 5$ K vs. field for 85.71% Fe_2O_3.

The saturation magnetization at 5 K is shown as function of composition in Fig. 8. The inset shows the M vs. H curve for $SrFe_{12}O_{19}$, the magnetization saturates at $H > 30$ kOe. The observed M_s of 101.3 emu/g corresponds to 19.3 μ_B. The measured M_s of the Sr- and Fe-excess compositions are somewhat smaller compared to that of $SrFe_{12}O_{19}$ since these materials contain additional, less magnetic phases. If the ferrite would be able to dissolve some SrO or Fe_2O_3 and form a limited range of solid solution we would expect a regular change of the saturation magnetization within the range of solubility.

3.3. Other hexagonal ferrites

The phase equilibrium studies (Section 3.1) have indicated that hexagonal ferrites with different structural stacking motifs exist in the pseudo-binary SrO–Fe_2O_3 system (Fig. 2a). We therefore attempted the synthesis of single-phase *W*- and *X*-type hexagonal Sr ferrites.

$SrFe_{18}O_{27}$ with *W*-type structure is stable only between 1350 and 1440 °C (Fig. 2a). Samples of that composition (set B) were sintered at 1400 °C for 24 h in air and quenched. Powder X-ray diffraction pattern of this material (Fig. 9a) were indexed within the hexagonal *W*-type structure (SG $P6_3/mmc$). The refined unit cell parameters are $a_0 = 5.8969(5)$ Å and $c_0 = 32.799(3)$ Å ($z = 2$). The sample was confirmed to be single-phase by scanning electron microscopy (Fig. 9a, inset).

$Sr_2Fe_{30}O_{46}$ with *X*-type hexagonal structure was also synthesized. Since the stability field of this compound was determined to be between 1350 and 1420 °C (Fig. 2a) a sample of set B with 88.2 mol% Fe_2O_3 was sintered at 1370 °C for 24 h in air and quenched. The sample was shown to be single-phase by powder X-ray diffraction and SEM (Fig. 9b). All diffraction peaks were completely indexed within the hexagonal *X*-type structure (SG: $R\bar{3}m$; $z = 3$). The refined lattice parameters are $a_0 = 5.8940(5)$ Å and $c_0 = 83.808(8)$ Å. The Fe^{2+} concentrations of both hexagonal ferrites were determined by titration. For $SrFe_2^{2+}Fe_{16}^{3+}O_{27}$ a Fe^{2+}-concentration of 6.06 ± 0.05 wt% was found (theoretical: 7.32%) and for *X*-type $Sr_2Fe_2^{2+}Fe_{28}^{3+}O_{46}$ (theoretical 4.32%) the Fe^{2+}-content was measured to be 3.42 ± 0.02 wt%. These data confirm a significant concentration of ferrous ions in both ferrites.

The thermal stabilities of *W*- and *X*-hexagonal ferrites were also studied by thermal analysis. The TG/DTA curves are shown in comparison to the *M*-type ferrite (details already discussed above)

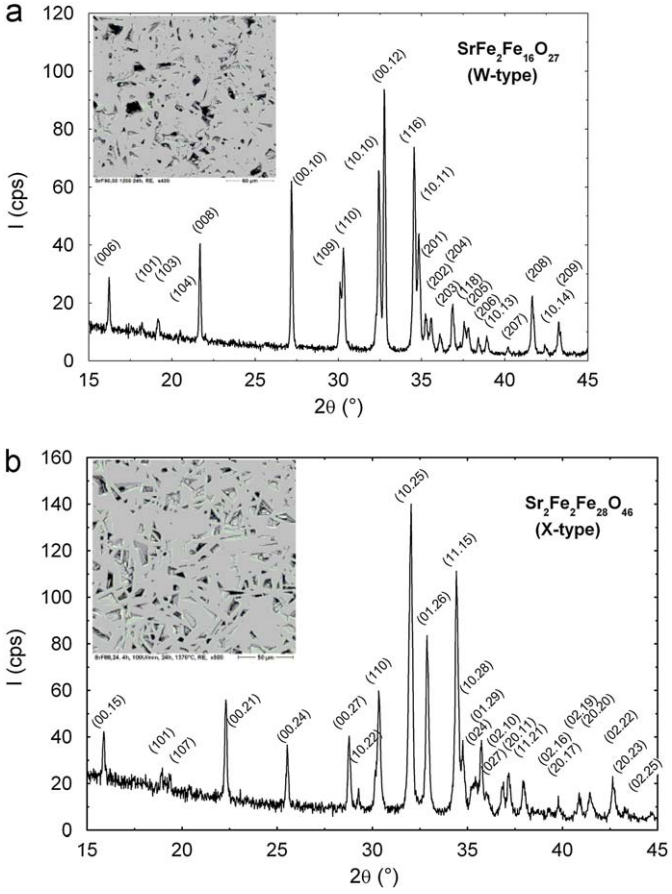

Fig. 9. X-ray diffraction patterns of (a) $SrFe_{18}O_{27}$ sintered at 1400 °C (inset: SEM micrograph) and of (b) $Sr_2Fe_{30}O_{46}$ sintered at 1370 °C (inset: SEM micrograph (grey: ferrite; dark: pores)).

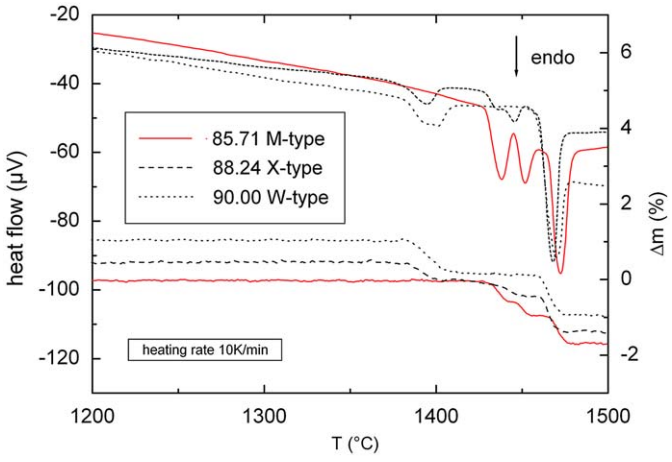

Fig. 10. Thermal analysis curves (TG and DTA) of hexagonal ferrites: *M*-type $SrFe_{12}O_{19}$, *W*-type $SrFe_{18}O_{27}$ and *X*-type $Sr_2Fe_{30}O_{46}$.

in Fig. 10. Since both *X*- and *W*-type are metastable at $T < 1350$ °C, the samples tend to decompose during heating. In both cases, a DTA peak with onset at 1365 °C and a mass loss indicates the reformation of the hexagonal ferrites according to

$$2SrFe_{12}^{3+}O_{19} + 3Fe_2O_3 \rightleftarrows Sr_2Fe_2^{2+}Fe_{28}^{3+}O_{46} + \tfrac{1}{2}O_2 \quad (1)$$

$$SrFe_{12}O_{19} + 3Fe_2O_3 \rightleftarrows SrFe_2^{2+}Fe_{16}^{3+}O_{27} + \tfrac{1}{2}O_2 \quad (2)$$

The experimental mass losses are 0.5% (theoretical 0.61%) and 1.0% (theoretical 1.04%) for reactions (1) and (2), respectively.

If the temperature is further raised, only two endothermic DTA peaks are observed for $Sr_2Fe_2Fe_{28}O_{46}$ (*X*-type); one at $T_{on} = 1423\,^{\circ}C$ for the incongruent melting of the *X*-type ferrite and another one at $T_{on} = 1443\,^{\circ}C$ for the incongruent melting of *W*-type ferrite. In accordance, a two step mass loss process is observed at $T > 1400\,^{\circ}C$ (compared to the three step mass loss for *M*-type). For $SrFe_{18}O_{27}$ (*W*-type) only one DTA peak with $T_{on} = 1447\,^{\circ}C$ and one mass loss step is observed at $T > 1400\,^{\circ}C$ which is an indication of the incongruent melting of the *W*-type compound and transformation into magnetite and liquid.

3.4. $Sr_4Fe_6O_{13\pm\delta}$

The phase diagram study (Section 3.1) has shown that the Sr-rich phase coexisting with $SrFe_{12}O_{19}$ at $T > 1150\,^{\circ}C$ is $Sr_4Fe_6O_{13\pm\delta}$. This material was shown to decompose by incongruent melting at 1250 °C. A sample (set B) with 42.86% Fe_2O_3 was sintered at 1200 °C for 2 days in air and quenched. X-ray diffraction showed the sample to be single-phase orthorhombic $Sr_4Fe_6O_{13\pm\delta}$ with lattice parameters $a_0 = 11.118(1)$ Å, $b_0 = 18.975(2)$ Å and $c_0 = 5.5843(4)$ Å (SG: Iba2, $z = 4$). The single-phase quality of the sample was checked by SEM. Thermal analysis (Fig. 11) shows one endothermic signal at $T_{on} = 1255\,^{\circ}C$ indicating the decomposition. This is accompanied by a small mass gain of $\Delta m = 0.1\%$ which could be due to a change in the non-stoichiometry δ of the material and/or formation of $SrFeO_{3-\delta}$.

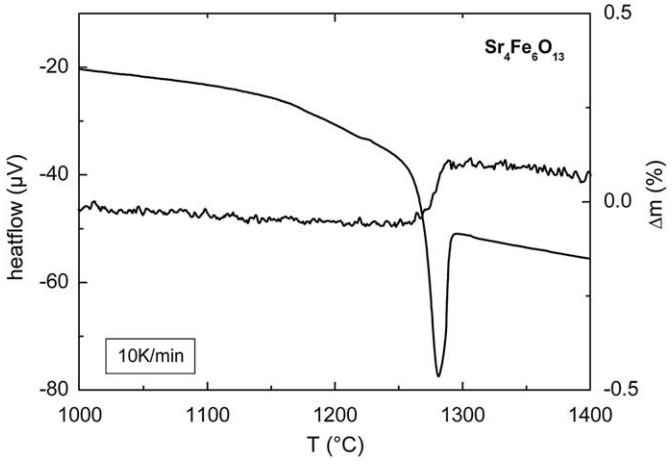

Fig. 11. Thermal analysis curves (TG and DTA) of $Sr_4Fe_6O_{13\pm\delta}$ sintered 48 h at 1200 °C.

4. Discussion

The results of this study of the Fe-rich part of the pseudo-binary system SrO–Fe_2O_3 at high temperatures ($T > 1150\,^{\circ}C$) in air are shown in Fig. 12. These results can be combined with those by Fossdal et al. [10] on the Sr-rich part of that system to give a combined phase diagram SrO–Fe_2O_3 in air. Liquidus lines were taken from Refs. [2,3,10]. Moreover, one has to take into consideration that our and Fossdal's [10] diagrams are based on experiments performed in air. The original data of Batti [2] on the SrO-rich part (<40 mol% Fe_2O_3) at $T > 1000\,^{\circ}C$ were measured in oxygen. The effect of the different partial pressures of oxygen (between oxygen and air) on the phase relations is assumed to be small.

The Fe-rich part of the system SrO–Fe_2O_3 is dominated by the existence of hexagonal ferrites. *M*-type $SrFe_{12}O_{19}$ does not have a significant solubility for SrO as proposed by Goto et al. [3]. The solubility of SrO is rather limited (85.71 ± 0.2 mol% Fe_2O_3). Consequently, Sr-hexaferrite compositions with SrO-excess represent two-phase mixtures of $SrFe_{12}O_{19}$ in equilibrium with $Sr_4Fe_6O_{13\pm\delta}$ at $T < 1206\,^{\circ}C$. Above 1206 °C, *M*-type ferrite is in equilibrium with a liquid phase up to the incongruent melting temperature of $SrFe_{12}O_{19}$ at 1410 °C.

$Sr_2Fe_{30}O_{46}$ is another equilibrium ferrite phase with *X*-type hexagonal ferrite structure. This compound is formed at 1350 °C according to Eq. (1) and decomposes at 1420 °C. Surprisingly, reports on Sr–*X* hexagonal ferrite hardly exist in the literature. It

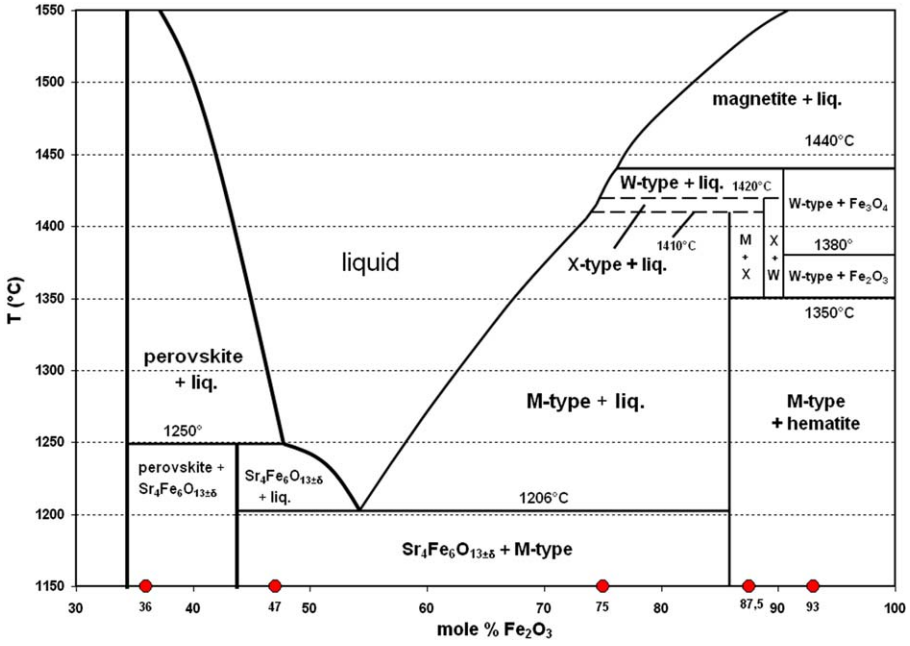

Fig. 12. Fe-rich part (>33 mol% Fe_2O_3) of the pseudo-binary phase diagram SrO–Fe_2O_3 in air (liquid compositions after Goto et al. [3]; starting mixtures SF included at the bottom (●)) ($M = SrFe_{12}O_{19}$, $W = SrFe_2^{2+}Fe_{16}O_{27}$, $X = Sr_2Fe_2^{2+}Fe_{28}O_{46}$, perovskite = $SrFeO_{3-\delta}$).

has also not been considered in any phase diagram study, although the analogous Ba–*X* ferrite appears as a stable phase in one diagram of the $BaO–Fe_2O_3$ system [13]. To the author's best knowledge, only the magnetic properties of Sr–*X* were described by Dey et al. [14], however, the sample was synthesized at 1250 °C therefore the quality of the sample and data is questionable (no XRD reported). Moreover, the disaccomodation behavior of Sr–*X* was studied, however, data on sample preparation and stability were not given [15]. Therefore, we report here for the first time the stability limits of $Sr_2Fe_{30}O_{46}$ in air. The measured saturation magnetization of 100.2 emu/g is in good agreement with Ref. [14].

$SrFe_{18}O_{27}$ with *W*-type hexagonal ferrite structure is formed at 1350 °C according Eq. (2). It is stable only up to 1440 °C. The saturation magnetization of 100.5 emu/g agrees with earlier reports [14]. Both, Sr–*X* and Sr–*W* ferrites contain significant concentrations of ferrous ions as confirmed by titrations. The large Fe^{2+}-concentrations seem to be the reason for the instability at lower temperatures: the reverse reactions (1) and (2) show that oxygen uptake and oxidation of Fe^{2+} with decreasing temperature leads to formation of *M*-type ferrite and haematite with ferric ions only. Therefore, reduction of the oxygen partial pressure should stabilize Sr–*X* and Sr–*W* at lower temperatures. The formation of other hexagonal ferrites, e.g. with M_3S, M_4S or M_6S hexagonal stacking variants was not observed.

In accordance with the findings by Fossdal et al. [10] we confirm that $Sr_4Fe_6O_{13\pm\delta}$ exists as a stable phase at intermediate temperature. This oxide incongruently melts at 1250 °C under formation of perovskite-type $SrFeO_{3-\delta}$ and a liquid phase.

5. Conclusions

A re-investigation of the Fe-rich part of the pseudo-binary system SrO–Fe_2O_3 (30–100 mol% Fe_2O_3) in air was performed. Due to contradictory data from earlier phase diagram studies we intended to clearly determine the phase relations of this system. We found that (i) *M*-type ferrite $SrFe_{12}O_{19}$ does not exhibit significant solubility for SrO and hence has a very limited phase field; (ii) the *X*-type ferrite $Sr_2Fe_{30}O_{46}$ and *W*-type ferrite $SrFe_{18}O_{27}$ are formed at 1350 °C and decompose in air at 1420 and 1440 °C, respectively; and (iii) $Sr_4Fe_6O_{13\pm\delta}$ is stable up to 1250 °C.

Acknowledgments

The authors thank Mrs. K. Franke (FHJ) for sample preparation and Mrs. M. Friedrich (FHJ) for SEM measurements. This work was supported by a grant (To165-3-2, Go606-7-1) from the Deutsche Forschungsgemeinschaft (DFG), Germany.

References

[1] J.J. Went, G.W. Rathenau, E.W. Gorter, G.W. van Oosterhout, Philips Tech. Rundsch. 13 (1952) 361–376.
[2] P. Batti, Ceramurgia 6 (1976) 11–16.
[3] Y. Goto, K. Takahashi, J. Jpn. Soc. Powder Metall. 17 (1971) 193–197.
[4] V. Adelsköld, Ark. Kemi. Minerali. Geol. 12 (a) (1938) 1–9.
[5] J. Smit, H.P.J. Wijn, Ferrites, Centrex Verlag, Eindhoven, 1962.
[6] M. Sugimoto, in: E.P. Wohlfahrt (Ed.), Ferromagnetic Materials, vol. 3, North-Holland Publ., Amsterdam, 1982, pp. 393–439.
[7] A. Yoshiasa, K. Ueno, F. Kanamaru, H. Horiuchi, Mater. Res. Bull. 21 (1986) 175–181.
[8] R. Bredesen, T. Norby, A. Bardal, V. Lynum, Solid State Ionics 135 (2000) 687–697.
[9] B. Mellenne, R. Retoux, C. Lepoittevin, M. Hervieu, B. Raveau, Chem. Mater. 16 (2004) 5006–5013.
[10] A. Fossdal, M.-A. Einarsrud, T. Grande, J. Solid State Chem. 177 (2004) 2933–2942.
[11] H. Kojima, in: E.P. Wohlfahrt (Ed.), Ferromagnetic Materials, vol. 3, North-Holland Publ., Amsterdam, 1982, pp. 305–391.
[12] X. Obradors, X. Solans, A. Collomb, D. Samaras, J. Rodriguez, M. Pernet, M. Font-Altaba, J. Solid State Chem. 72 (1988) 218–224.
[13] H.J. van Hook, J. Am. Ceram. Soc. 47 (1964) 579.
[14] S. Dey, R. Valenzuela, J. Appl. Phys. 55 (1984) 2340–2342.
[15] P. Hernandez-Gomez, P. Bercoff, O. Alejos, C. Torres, J.M. Munoz, C. de Francisco, J. Iniguez, H. Bertorello, Physica B 320 (2002) 267–269.
[16] M. Okrusch, S. Matthes, Eine Einführung in die spezielle Mineralogie, Petrologie und Lagerstättenkunde (in german), vol. 7, Springer Verlag, Berlin, 2005 Auflage 477.